ELSEVIER

International Journal of Heat and Fluid Flow 20 (1999) 414–421

International Journal of HEAT AND FLUID FLOW

www.elsevier.com/locate/ijhff

A numerical study of steady viscous flow past a fluid sphere

Gh. Juncu [1]

Politehnica University Bucharest, Catedra Inginerie Chimica, Polizu 1, 78126 Bucharest, Romania

Received 15 July 1998; accepted 9 January 1999

Abstract

This paper presents a computational study of the steady viscous flow of a fluid over a spherical drop or bubble of another immiscible fluid. Numerical solutions have been obtained for external Reynolds numbers up to 500. The range of viscosity ratio is from 0.01 to 100.0. The density ratio varies between the same limits. The finite difference method was employed to discretize the model equations. A nested DC algorithm solved the nonlinear algebraic systems. Flow separation, the effect of internal Re number on the flow pattern and the computations of the drag coefficients are analysed. Vortex, velocity and pressure distributions on the drop surface are presented. The values obtained for drag coefficients are compared with the solutions provided by published predictive equations.

Keywords: Navier–Stokes equations; Fluid sphere; Defect correction

1. Introduction

The phenomena of momentum, heat and mass transport between a translating drop or bubble and its surrounding fluid have been investigated intensively due to a wide range of industrial and scientific applications. The problem is classified as:

"external" – if the transfer resistance is assumed negligible inside the drop as compared to that of continuous phase;

"internal" – if the transfer resistance in the continuous phase is assumed negligible as compared to that inside the drop, and

"conjugate" – if the transfer resistance in both phases is comparable to each other.

The literature contains few theoretical solutions of the conjugate momentum transfer from the fluid particle for intermediate values of the viscosity ratio of the two phases. Most reported results refer to the limits in which the viscosity ratio is either very small or very large. Clift et al. (1978), Oliver and Chung (1985, 1987) and Sadhal et al. (1996) review these studies.

For $Re \geqslant 1$, the most complete and reliable solutions of the Navier–Stokes equations for the flows inside and around a fluid sphere are given by numerical methods. Oliver and Chung (1985, 1987) discuss the limits of the Galerkin and boundary layer solutions. Abdel-Alim and Hamielec (1975), for steady-state flow at $Re \leqslant 50$, viscosity ratio comprised between 0.0995 and 1.40 and density ratio of the two phases approximately equal to one, reported the earliest numerical solution. The discretization method used was the centred finite difference scheme. The resultant nonlinear discrete system was solved with a quasi-local – relaxation method with an empirical formula for the relaxation parameter. Rivkind et al. (1976) extended the work of Abdel-Alim and Hamielec to higher Re numbers (up to 100). The discretization scheme employed was the same. In the external field, the perturbation of stream function instead of the stream function (see also Cliffe and Lever, 1986) was used. The method of variable directions was used to solve the nonlinear discrete system. With the same numerical method Rivkind and Ryskin (1976) obtained solutions for exterior Re up to 200 and arbitrary values of the viscosity ratio. Oliver and Chung (1985, 1987) investigated the steady flows inside and around a fluid sphere at low Re numbers ($Re \leqslant 1$) (Oliver and Chung, 1985) and moderate Re numbers ($Re \leqslant 50$) (Oliver and Chung, 1987) using a hybrid method which combines the series truncation techniques with finite differences (Oliver and Chung, 1985) or the cubic finite element method (Oliver and Chung, 1987).

Clift et al. (1978) stated that "for drops and bubbles rising or falling freely in systems of practical importance, significant deformations from the spherical occur for all $Re > 600$". The shape of the drop or bubble remains spherical if the Weber number is small enough ($We \leqslant 0.1$, Wellek et al., 1966; for more details, see Clift et al., 1978). In the studies mentioned previously, the exterior Re number $Re_2 = 200$ appears to be the upper limit for which complete, steady-state, flow fields have been reliably determined. There are many reasons for the continuing interest in this problem and in attempts to carry numerical calculations to still higher Reynolds numbers. The aim of this paper is to extend the domain of investigation for exterior Re up to 500. At each value of the exterior Re number, the influence of the viscosity and density ratios on the flow patterns and drag coefficients is analysed. A numerical procedure, which emerges to be very simple, robust and efficient, is presented.

[1] Tel.: +40 1 312 6879; fax: +40 1 312 6879; e-mail: juncu@cael.pub.ro

0142-727X/99/$ – see front matter
PII: S0142-727X(99)00003-X

2. Model equations

Consider a fluid sphere of radius a moving into an unbounded volume of another immiscible fluid. The following assumptions are considered valid:

(i) the fluids are Newtonian;
(ii) the flows are steady, axisymmetric and laminar;
(iii) the physical properties (density – ρ and viscosity – ν) of the particle and medium are constant;
(iv) the shape of the particle remains spherical;
(v) there is no interfacial mass transfer (the radial velocity is zero at interface);
(vi) there are no surface-active materials.

Under these assumptions, the dimensionless Navier–Stokes equations, expressed in dimensionless stream-function and vorticity in spherical coordinate system (r,θ), are:

- The interior flow field

$$\left[\frac{\partial \Psi_1}{\partial r}\frac{\partial}{\partial \theta}\left(\frac{\zeta_1}{r\sin\theta}\right)-\frac{\partial \Psi_1}{\partial \theta}\frac{\partial}{\partial r}\left(\frac{\zeta_1}{r\sin\theta}\right)\right]\sin\theta = \frac{2}{\mathrm{Re}_1}E^2(\zeta_1 r\sin\theta), \tag{1a}$$

$$E^2(\Psi_1)-\zeta_1 r\sin\theta = 0, \tag{1b}$$

where

$$E^2=\frac{\partial^2}{\partial r^2}+\frac{\sin\theta}{r^2}\frac{\partial}{\partial\theta}\left(\frac{1}{\sin\theta}\frac{\partial}{\partial\theta}\right),\quad \mathrm{Re}_1=UD\rho_1/\nu_1,$$

$$D=2a.$$

- The exterior flow field

$$\frac{\mathrm{Re}_2}{2}\left[\frac{\partial}{\partial\theta}(\mathrm{e}^z V_{\theta,2}\zeta_2)+\frac{\partial}{\partial z}(\mathrm{e}^z V_{\mathrm{R},2}\zeta_2)\right] = \frac{\partial^2\zeta_2}{\partial z^2}+\frac{\partial^2\zeta_2}{\partial\theta^2}+\frac{\partial\zeta_2}{\partial z}+\cot\theta\frac{\partial\zeta_2}{\partial\theta}-\frac{\zeta_2}{\sin^2\theta}, \tag{2a}$$

$$\frac{\partial^2\Psi_2}{\partial z^2}+\frac{\partial^2\Psi_2}{\partial\theta^2}-\frac{\partial\Psi_2}{\partial z}-\cot\theta\frac{\partial\Psi_2}{\partial\theta}=\zeta_2\mathrm{e}^{3z}\sin\theta, \tag{2b}$$

where

$$V_{\mathrm{R},2}=-\frac{1}{\mathrm{e}^{2z}\sin\theta}\frac{\partial\Psi_2}{\partial\theta},\quad V_{\theta,2}=\frac{1}{\mathrm{e}^{2z}\sin\theta}\frac{\partial\Psi_2}{\partial z},$$

$$\mathrm{Re}_2=UD\rho_2/\nu_2,$$

In Eqs. (2a) and (2b) the well-known transformation $r=\exp z$ was applied. The boundary conditions to be satisfied are:

- At the sphere centre $(r=0)$

$$\Psi_1=\zeta_1=0. \tag{3a}$$

- At the interface $(r=1,\ z=0)$

$$V_{\theta 1}=V_{\theta 2},\ \text{continuity of tangential velocity}, \tag{3b}$$

$$V_{\mathrm{R}1}=V_{\mathrm{R}2}=0,\ \text{no mass transfer across the interface}, \tag{3c}$$

$$\nu_1(\zeta_1-2V_{\theta 1})=\nu_2(\zeta_2-2V_{\theta 2}),\ \text{equal shear stress}, \tag{3d}$$

$$\Psi_1=\Psi_2=0. \tag{3e}$$

- At free stream $(z=\infty)$

$$\Psi_2=\frac{1}{2}z^2\sin^2\theta,\quad \zeta_2=0.0. \tag{3f}$$

- At the symmetry axis $(\theta=0,\pi)$

$$\Psi_i=\zeta_i=0,\quad i=1,2. \tag{3g}$$

The velocities are nondimensionalized by the free-stream velocity U, the stream function Ψ by Ua^2 and the radial coordinate by a. The dimensionless vorticity is defined by:

$$\zeta_1=\frac{1}{r}\frac{\partial V_{\mathrm{R},1}}{\partial\theta}-\frac{\partial V_{\theta,1}}{\partial r}-\frac{V_{\theta,1}}{r},$$

$$\zeta_2=\frac{1}{\mathrm{e}^z}\left(\frac{\partial V_{\mathrm{R},2}}{\partial\theta}-\frac{\partial V_{\theta,2}}{\partial z}-V_{\mathrm{R},2}\right), \tag{4}$$

where

$$V_{\mathrm{R},1}=-\frac{1}{r^2\sin\theta}\frac{\partial\Psi_1}{\partial\theta},\quad V_{\theta,1}=\frac{1}{r\sin\theta}\frac{\partial\Psi_1}{\partial r}.$$

The results of interest are usually expressed by the interface tangential velocity and vorticity, the surface pressure, the drag coefficients and the vortex length. The surface pressure and the drag coefficients were calculated using the following relations:

- Surface pressure

$$P_{\mathrm{s}}(\theta)=P_0+\frac{4}{\mathrm{Re}_2}\int_0^\theta\left(\frac{\partial\zeta_2}{\partial z}+\zeta_2\right)_{z=0}\mathrm{d}\theta-V_{\theta,\mathrm{s}}^2,$$

$$P_0=1+\frac{8}{\mathrm{Re}_2}\int_0^\infty\left(\frac{\partial\zeta_2}{\partial\theta}\right)_{\theta=0}\mathrm{d}z. \tag{5a}$$

- Pressure drag coefficient

$$C_{\mathrm{DP}}=\int_0^\pi P_{\mathrm{s}}\sin 2\theta\,\mathrm{d}\theta. \tag{5b}$$

- Friction drag coefficient

$$C_{\mathrm{DF}}=\frac{8}{\mathrm{Re}_2}\int_0^\pi\zeta_{2,\mathrm{s}}\sin^2\theta\,\mathrm{d}\theta. \tag{5c}$$

- Total drag coefficient

$$C_{\mathrm{D}}=C_{\mathrm{DP}}+C_{\mathrm{DF}}. \tag{5d}$$

3. Solution procedure

The first step of the numerical solving of the system (1)–(3) is the choice of the discretization scheme. For convection-dominated convection – diffusion equations, the widely used methods are finite differences, finite element and spectral collocation. In this work finite differences were used.

The finite differences discrete approximation of the model equations is a large, sparse, nonlinear algebraic system. The efficient solving of this system is done by iterative methods. To accurately predict the flow, a scheme with at least second order accuracy must be used. For convection-dominated convection – diffusion equations, second order differencing of the convective derivative causes numerical instabilities, unless the method grid size is very small. Three of the methods used to overcome these problems are discussed below. In the first, the centred difference scheme is employed for discretization and the local relaxation algorithm (Botta and Veldman, 1981) to solve the discrete system. Also, the "correction term" algorithm (Fasel, 1977), is considered a local relaxation-like method by Botta and Veldman (1981). The second variant, the defect correction (DC) algorithm (Stetter, 1978), employs a double discretization combined with a double iterative method. The third variant is the high order compact scheme developed by Gupta et al. (1984).

Too much experience in solving numerically the conjugate momentum transfer from a fluid particle is not available. The Hamielec school uses a quasi-local relaxation method. Rivkind et al. (1976) offer few details about the numerics. The methods employed by Oliver and Chung (1985, 1987) are outside the subject of this section. To select one of the previous methods,

the experience accumulated in solving the flow past a rigid sphere may be a starting point.

A specific problem of the local relaxation algorithms is the computation of the relaxation parameter for the surface vorticity. This parameter cannot be calculated according to the rules used at the interior grid points. A trail procedure should be used. The tests made (Juncu and Mihail, 1989) showed that there is an optimal, mesh-dependent value of this parameter and the number of iterations depends strongly on this value. The compact schemes lead to a nine-point stencil using laborious relations to compute the discretization coefficients. Also, these schemes are not as general as the usual differences schemes. In these conditions, from our experiences and knowledge, the method that emerges as the most robust is DC.

Denote by $N_{h,1}$ and $N_{h,2}$ the first order accurate, respectively, the second order accurate discretization of the nonlinear Eqs. (1a) and (1b) and Eqs. (2a) and (2b). The DC iteration may be written as

$$N_{h,1}(u_h^{i+1} - u_h^i) = R_{h,2}, \tag{6}$$

where $R_{h,2}$ is the residual of the second order discretization, u_h^i is the discrete approximation of the solution after i iterations on the mesh with step size h. The starting approximation u_h^1 is the first order accurate solution. A DC step needs solving the nonlinear system (6). The practice of the DC iteration shows that one or more steps of a given nonlinear iterative method can replace the exact solving of Eq. (6). The widely used iterative method is multigrid (MG) Hackbusch (1985). Some numerical experiments made by Juncu and Mihail (1990) showed that a single grid (SG) iterative method used inside a DC step performs quite acceptably. The combination defect correction–single grid (DC–SG) is considerably simpler to program and seems to be more versatile in comparison with the DC–MG algorithm.

The method used in this work is a nested DC–SG algorithm. The vorticity Eqs. (1a) and (2a) were discretized by the first order upwind scheme. The stream function Eqs. (1b) and (2b) were discretized by the centred second order accurate scheme. The boundary condition (3d) was solved in the manner presented by Rivkind et al. (1976). The value assigned to the relaxation coefficient was in all cases one.

The maximum number of levels used is 5. The coarsest has 17×17 points in each phase while the finest has 257×257 points in each phase. Point and alternating lines Gauss–Seidel methods (PGS and ALGS) were used as SG iterations. The number of PGS or ALGS iterations used inside a DC step was varied between:

- PGS → (10, 50)
- ALGS → (5, 25)

The initial values on the coarsest grid for stream function and vorticity in both phases were set equal to zero on all grid points except for stream function at $z = \infty$ where the boundary condition (3f) holds.

All the computations were made on an HP 9000 series 715/80 work station in FORTRAN double precision.

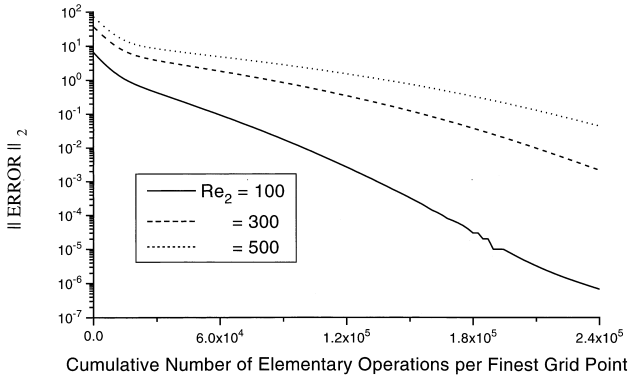

Fig. 1. The influence of the exterior Reynolds number, Re_2, on the DC–SG algorithm convergence rate; $\Phi_v = \Phi_\rho = 1.0$; 129×129 points mesh.

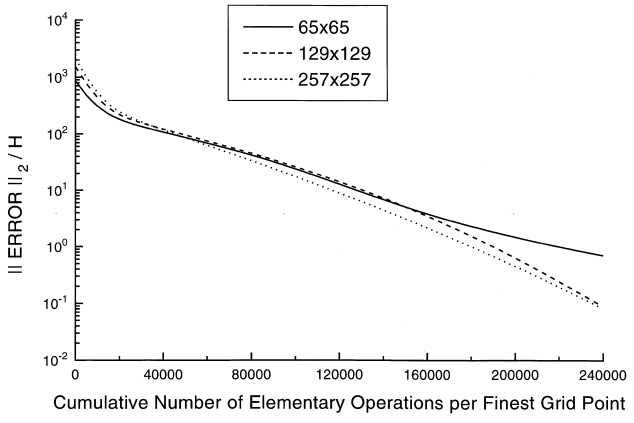

Fig. 2. Mesh behaviour of the algorithm at $Re_2 = 300$, $\Phi_v = \Phi_\rho = 1.0$.

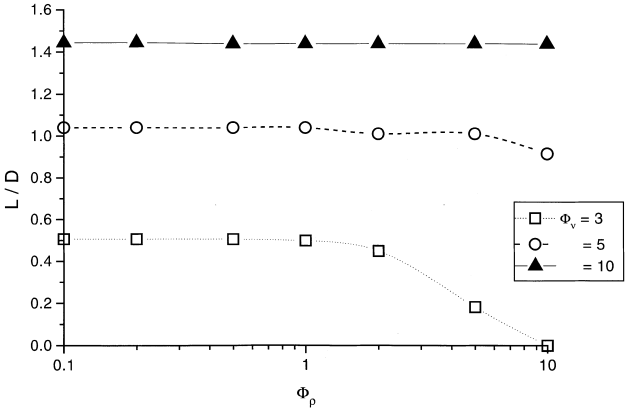

Fig. 3. Vortex length at $Re_2 = 100$.

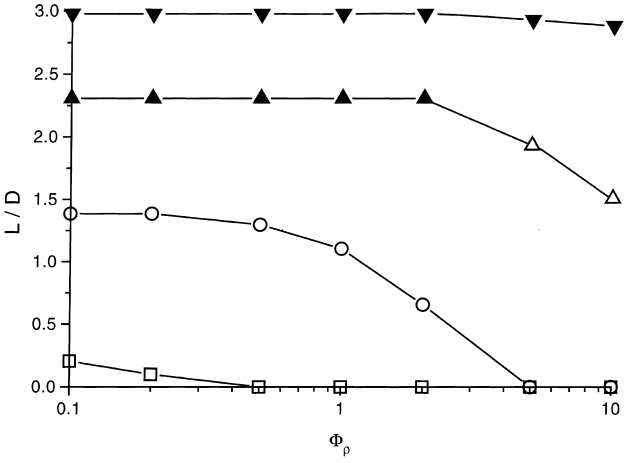

Fig. 4. Vortex length at $Re_2 = 300$; □–$\Phi_v = 2$; ◯–$\Phi_v = 3$; Δ–$\Phi_v = 5$; $\Phi_v = 10$.

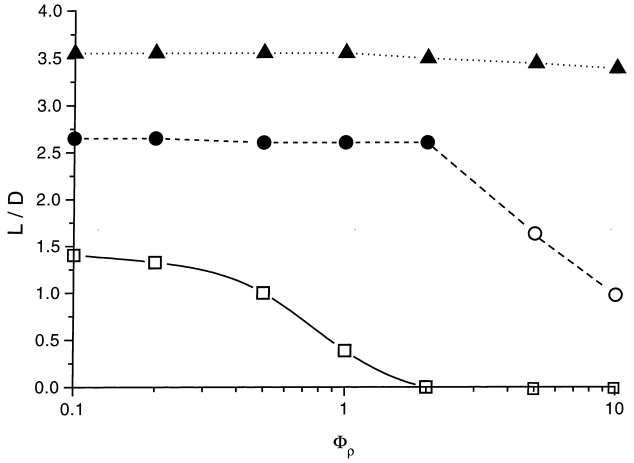

Fig. 5. Vortex length at $Re_2 = 500$; □–$\Phi_v = 3$; ○–$\Phi_v = 5$; $\Phi_v = 10$.

4. Results

First, some results concerning the numerical performances of this algorithm are briefly presented. The algorithm converged for all Re number values used in this work. The numerical results presented refer to the Re_2 influences on the convergence rate and the algorithm mesh behaviour. The influence of the inner iterations number on the convergence rate may be predicted from the theorems of Auzinger and Stetter (1982).

The convergence rate of the algorithm function of Re_2 for $\Phi_v = v_1/v_2 = 1$ and $\Phi_\rho = \rho_1/\rho_2 = 1$ is presented in Fig. 1. The results plotted in Fig. 1 were obtained on a mesh having 129×129 points in each phase. The mesh behaviour of the algorithm at $Re_2 = 300$, $\Phi_v = 1$ and $\Phi_\rho = 1$ is presented in Fig. 2. Before discussing the results presented in Figs. 1 and 2 it must be mentioned that the results provided by the two inner iterative methods (PGS and ALGS), coincide at the same number of elementary operations per grid point. Also, the influence of the physical properties ratios, Φ_v and Φ_ρ, on the convergence rate is not noticeable.

Fig. 1 shows that, as expected, the convergence rate of the algorithm decreases with the increase in Re_2. Fig. 2 shows that, for a given Re_2, the convergence rate of the algorithm is mesh-dependent and the operation count is approximately $\mathcal{O}(N)^{1.5}$. This result may be considered quite satisfactory.

The controlling parameters of the problem are: Re_2, Φ_v and Φ_ρ. The internal phase Reynolds number, Re_1, may be expressed as: $Re_1 = Re_2\Phi_\rho/\Phi_v$. The values of Φ_v and Φ_ρ were chosen to reproduce the real systems. For a liquid–liquid system, both liquids being Newtonian, the interval [0.10, 10.0] covers the values of practical interest for Φ_v and Φ_ρ. To complete the analysis with values typical for gas–liquid

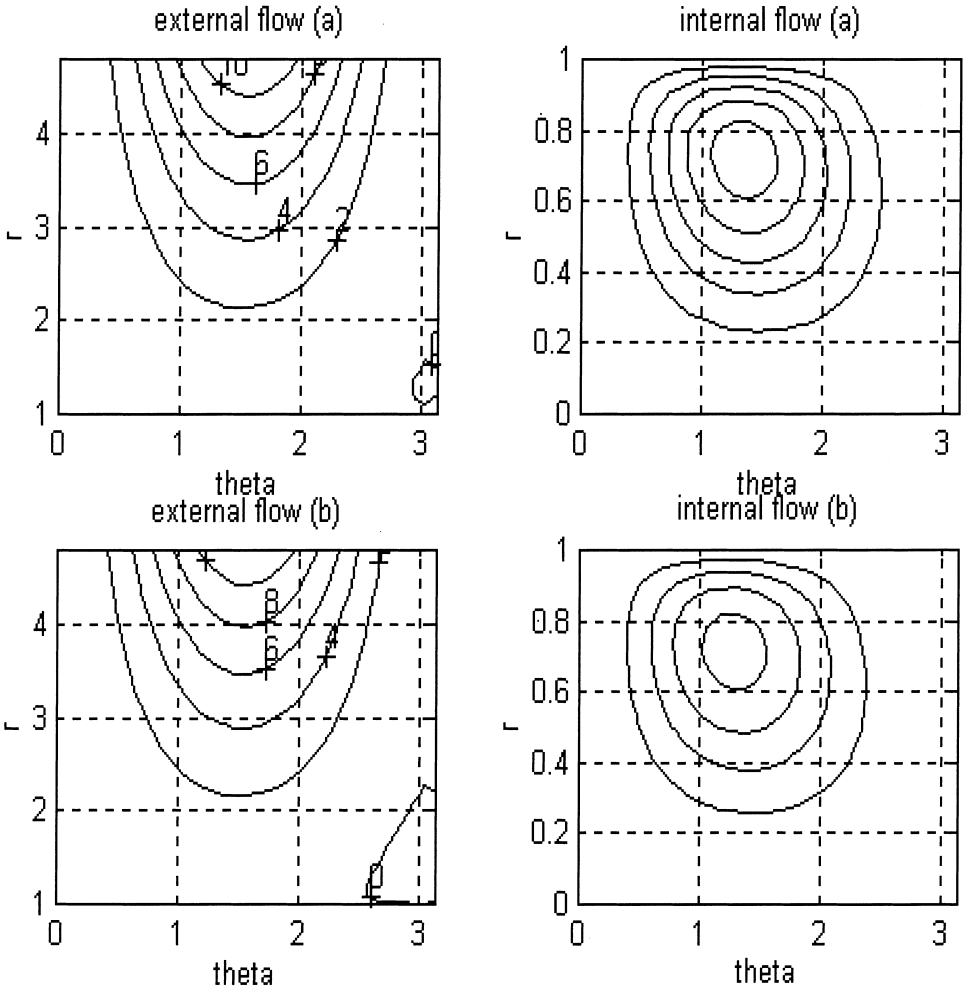

Fig. 6. Stream function contours at $Re_2 = 100$ and $\Phi_\rho = 1.0$. (a) $\Phi_v = 3.0$; (b) $\Phi_v = 10.0$.

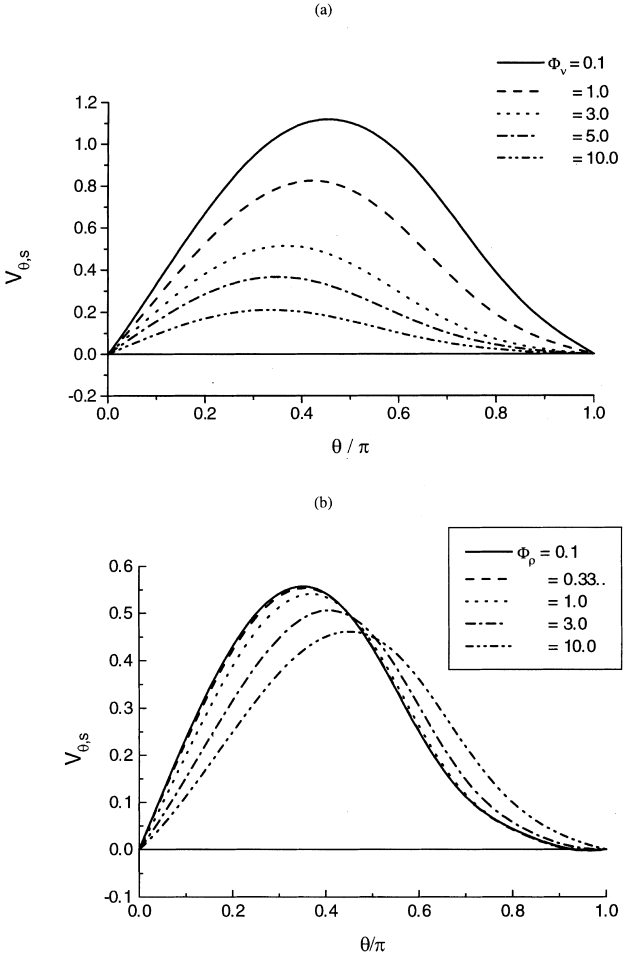

Fig. 7. The Φ_v and Φ_ρ influence on the interface tangential velocity: (a) $Re_2 = 100$, $\Phi_\rho = 1.0$; (b) $Re_2 = 300$, $\Phi_v = 5.0$.

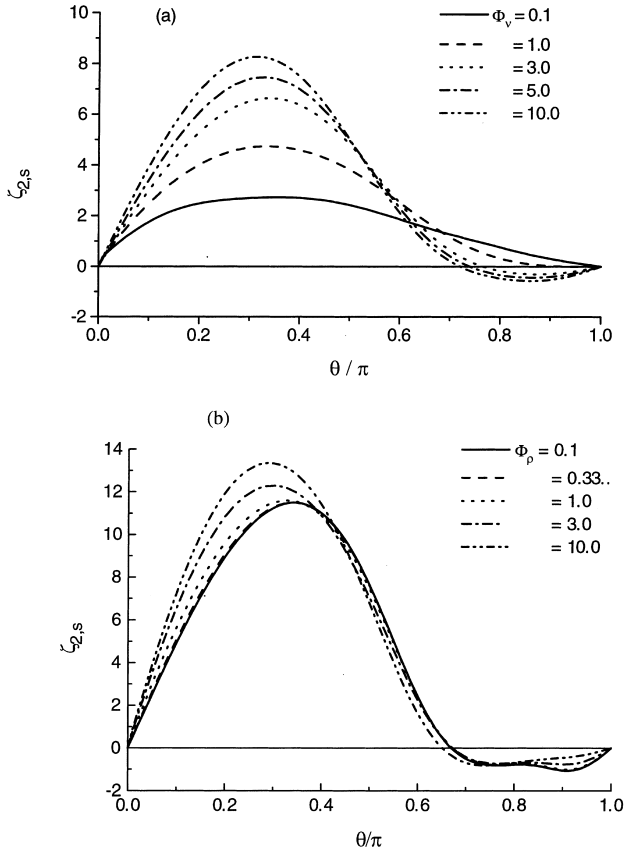

Fig. 8. The Φ_v and Φ_ρ influence on the exterior interface vorticity, $\zeta_{2,s}$; (a) $Re_2 = 100$, $\Phi_\rho = 1.0$; (b) $Re_2 = 300$, $\Phi_v = 5.0$.

systems, two additional sets of Φ_v and Φ_ρ values, $\Phi_v = \Phi_\rho = 0.01$ and $\Phi_v = \Phi_\rho = 100.0$ were added.

Rivkind and Ryskin (1976) identify three main problems in studying the flow past a fluid sphere. The first refers to the flow return behind drop. The second analyses the effect of internal Re number, Re_1, on the flow. The third is the computation of the drag coefficient of the drop. The same way was followed in this work. Three values of Re_2, $Re_2 = 100$, 300 and 500 are considered. At each Re_2 value, the Φ_v and Φ_ρ influence on flow patterns and the drag coefficient is analysed. The results presented at $Re_2 = 100$ were obtained on a mesh with 129×129 points in each phase. The results presented at $Re_2 = 300$ and 500 were obtained on the mesh with 237×257 points in each phase.

Due to the presence of velocity at the interface of the two fluids, the separation point is the point where the velocity becomes zero, and not the point of zero tangential stress, as in the case of flow over a solid particle. Calculations made by Rivkind et al. (1976) and Rivkind and Ryskin (1976) show that, if the viscosity ratio does not exceed 1, the flow around the drop does not separate and there is no return-flow region behind the drop. Another new aspect presented by Rivkind and Ryskin (1976) is the return flow behind the body without

Table 1
The drag coefficient at $Re_2 = 100$

Φ_v	Φ_ρ									Eq. (7)
	0.01	0.1	0.2	0.5	1.0	2.0	5.0	10.0	100.0	
0.01	0.384	–	–	–	–	–	–	–	–	0.417
0.1	–	0.421	0.421	0.422	0.423	0.425	0.427	0.430	–	0.473
0.2	–	0.461	0.461	0.462	0.462	0.464	0.464	0.466	–	0.526
0.5	–	0.558	0.558	0.558	0.559	0.560	0.562	0.566	–	0.641
1.0	–	0.676	0.676	0.676	0.674	0.670	0.667	0.665	–	0.756
2.0	–	0.812	0.812	0.812	0.811	0.810	0.807	0.799	–	0.871
3.0	–	0.883	0.883	0.883	0.882	0.881	0.875	0.867	–	0.929
5.0	–	0.951	0.951	0.951	0.951	0.951	0.948	0.944	–	0.987
10.0	–	1.008	1.008	1.008	1.008	1.008	1.008	1.007	–	1.04
100.0	–	–	–	–	–	–	–	–	1.06	1.095

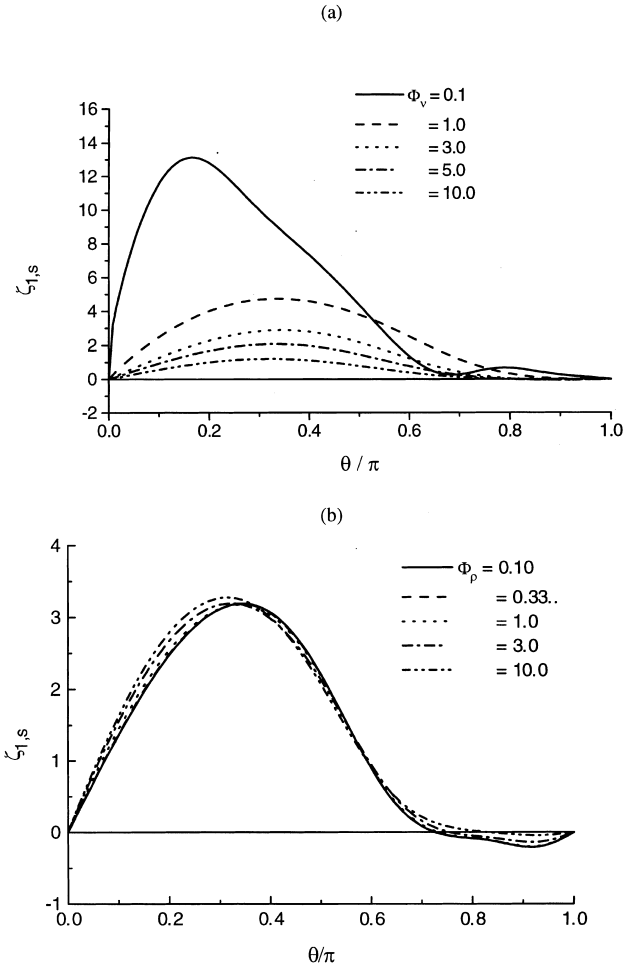

Fig. 9. The Φ_v and Φ_ρ influence on the interior interface vorticity: $\zeta_{1,s}$; (a) $Re_2 = 100$, $\Phi_\rho = 1.0$; (b) $Re_2 = 300$, $\Phi_v = 5.0$.

separation (see also Clift et al., 1978, pp. 126). In this case the return-flow region is not contiguous with the drop surface. Rivkind and Ryskin (1976) mentioned also experimental confirmations of this phenomenon. For brevity, such a vortex is named here as fluid vortex while the vortex attached to the drop surface is named solid vortex.

The computations made confirm and complete the results of Rivkind and Ryskin (1976). The dimensionless vortex length, L/D, is plotted in Figs. 3–5. The solid symbols refer to solid vortex while the hallow symbols to fluid vortex. Figs. 3–5 show that flow separation occurs only if $\Phi_v > 5$ at $Re_2 = 100$ and $\Phi_v > 3$ at $Re_2 = 300$ and 500. The flow separation is influenced by the Φ_ρ value. At $\Phi_v = 2$ there is flow return behind the drop without separation only at $Re_2 = 300$ and $\Phi_\rho = 0.1$ and 0.2. The results obtained at $\Phi_v = 3$, 5 and 10 may be summarized as follows

$\Phi_v = 3$. Flow return behind the drop without flow separation was detected. The fluid vortex dimension depends on the Φ_ρ value. The increase in Re_1 decreases the fluid vortex length. At $Re_2 = 100$ and $\Phi_\rho = 10$, there is no flow return behind the drop. At $Re_2 = 300$, the fluid vortex disappears if $\Phi_\rho > 5$ while, at $Re_2 = 500$, the fluid vortex occurs if $\Phi_\rho < 2$.

$\Phi_v = 5$. For $Re_2 = 100$ only fluid vortex occurs for all $\Phi_\rho \in [0.1,\ 10.0]$. The fluid vortex length is not significantly affected by Φ_ρ. For $Re_2 = 300$ and 500 the vortex is attached if $\Phi_\rho < 5$ and detached if $\Phi_\rho > 2$. At $Re_2 = 300$ and 500, the solid vortex length is not influenced significantly by Φ_ρ.

$\Phi_v = 10$. Only solid vortex occurs. The density ratio has a negligible influence on the vortex length.

Usually, the results obtained at the flow past a drop at $\Phi_v \gg 1$ are compared with those obtained at the flow past a solid sphere. The value obtained here for the solid vortex length at $\Phi_v = \Phi_\rho = 100$ and $Re_2 = 100$ ($L/D = 1.669$) is higher than the vortex length obtained at the flow past a solid sphere at $Re_2 = 100$ ($L/D = 0.93$, Juncu and Mihail, 1990). At $Re_2 = 300$ and 500, steady numerical results for the flow past a solid sphere are not available. The L/D values obtained at $\Phi_v = \Phi_\rho = 100$ are:

$$Re_2 = 300, \quad L/D = 3.496;$$
$$Re_2 = 500, \quad L/D = 4.08.$$

The influence of a given parameter on the flow patterns is usually expressed by the values of the surface tangential velocity, vorticity and pressure. Graphical presentation of the stream function and/or vorticity contours is also useful. The influence of Φ_v and Φ_ρ on the stream function contours, surface velocity, vorticity and pressure is given in Figs. 6–10. The symbols in Figs. 7–10 indicate the values of Φ_v (sub-figures (a)) or Φ_ρ (sub-figures (b)). Fig. 6(a) shows the streamlines when a fluid vortex is present. Fig. 6(b) plots the streamlines for the flow with separation.

At $Re_2 = 100$ the tangential surface velocity does not cross the zero axis for $0 < \theta < \pi$. The contact between the solid vortex and the drop surface occurs in a single point, at $\theta \cong \pi$. Negative values of the surface tangential velocity occurs only at $Re_2 > 100$. Fig. 7 shows that, at a given Re_2 value, the influence of Φ_v on V_θ is more significant in comparison with the Φ_ρ influence. The increase in Φ_v decreases the circulation inside the drop. The magnitude of the interface tangential velocity is not affected significantly by the variation in Φ_ρ. The decrease in Φ_ρ increases the asymmetry of the interface velocity. Negative values of the interface tangential velocity occur for Φ_ρ smaller than two, $Re_2 > 100$ and $\Phi_v > 3$. Figs. 8 and 9 plot the Φ_ρ and Φ_v influence on the vorticity computed on both sides of the interface. The increase in Φ_v decreases $\zeta_{1,s}$ and increases $\zeta_{2,s}$. The influence of Φ_ρ on $\zeta_{1,s}$ and $\zeta_{2,s}$ is less significant. Figs. 8 and 9 show negative values of the surface vorticities without flow separation. Fig. 10(a) shows that the surface pressure is affected by the variation of Φ_v. Fig. 10(b) shows that the influence of Φ_ρ on the surface pressure may be considered negligible.

Another interesting phenomenon presented by Rivkind and Ryskin (1976) is the break-up of internal circulation. This phenomenon occurs if $\Phi_\rho \gg \Phi_v$ and $\Phi_v > 1$ (flow separation exists in the external flow). The values employed in this work for Φ_ρ and Φ_v do not fulfil the conditions of internal flow break-up. For this reason, this phenomenon is not analysed here.

The calculated values of the drag coefficient at $Re_2 = 100$ are given in Table 1. The last column of Table 1 shows the values computed with the relation proposed by Rivkind and Ryskin (1976).

$$C_D = \frac{1}{1+\Phi_v}\left[\Phi_v\left(\frac{24}{Re_2} + 4Re_2^{(-1/3)}\right) + 14.9Re_2^{-0.78}\right]. \tag{7}$$

Oliver and Chung (1987) make the comparison between the values provided by relation (7) and the other values (experimental or theoretical) available in the literature. Table 1 shows that the Φ_ρ influence on C_D may be considered negligible. At a given Φ_v value, the drag coefficient variation function of the density ratio does not exceed 3%. The relative error between the present results and those of relation (7) is maximum 14%. The C_D values computed here are smaller than those provided by relation (7). The C_D value obtained in this work at $\Phi_v = 100$ agrees well with the C_D value ($C_D = 1.069$, Juncu and Mihail, 1990) for the flow past a solid sphere.

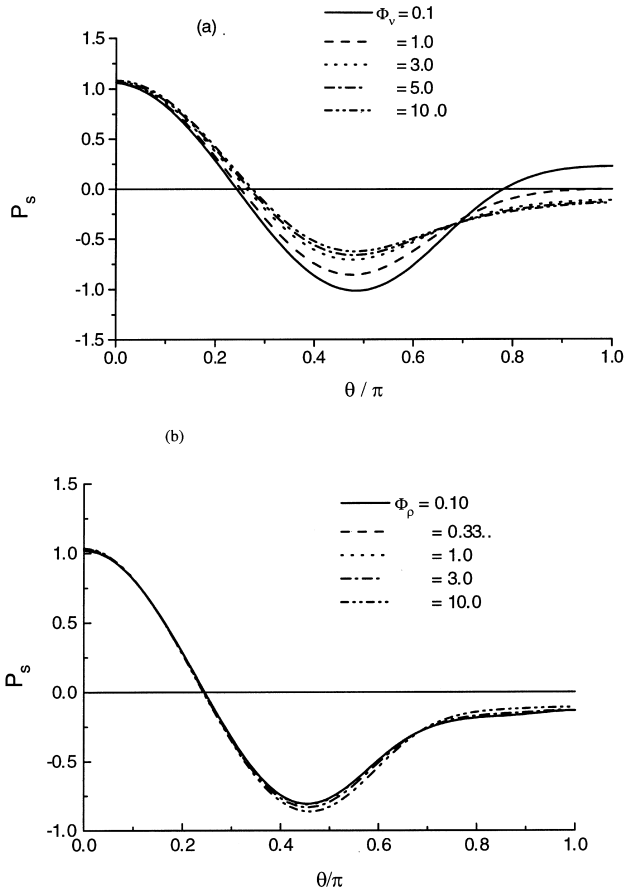

Fig. 10. The Φ_v and Φ_ρ influence on the interface pressure: (a) $Re_2 = 100$, $\Phi_\rho = 1.0$; (b) $Re_2 = 300$, $\Phi_v = 5.0$.

At $Re_2 = 300$ and 500 the influence of the density ratio on the drag coefficient is the same. For this reason, C_D is presented only graphically as function of Φ_v in Figs. 11 and 12. The dot curves show the values predicted by relation (7). Figs. 11 and 12 show that the disagreement between the present results and those provided by relation (7) increases with the increase in Re_2. As in the case $Re_2 = 100$, the present results are smaller than those of relation (7). However, before

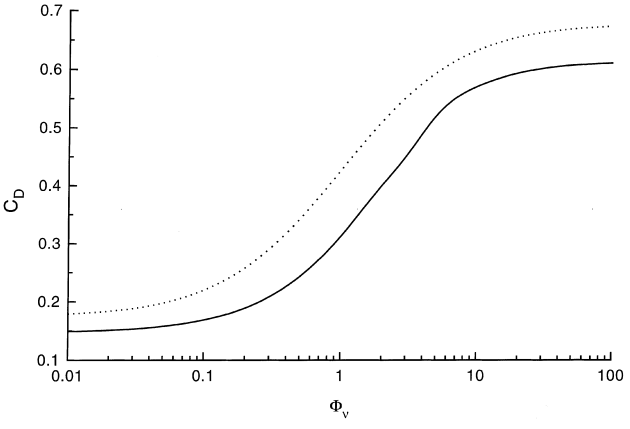

Fig. 11. Drag coefficient values at $Re_2 = 300$; —— present results; · · · relation (7).

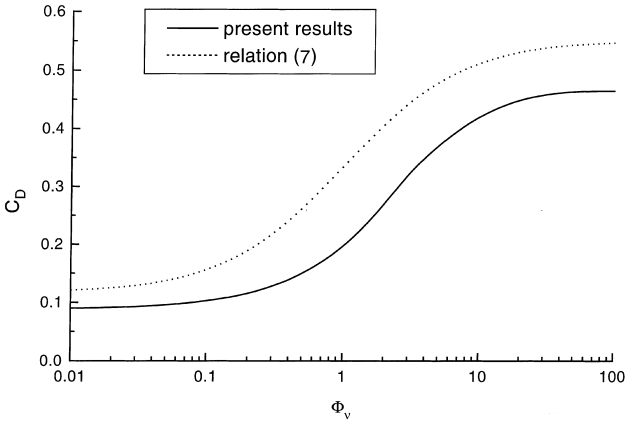

Fig. 12. Drag coefficient values at $Re_2 = 500$.

concluding about the validity of relation (7), the following aspects must be taken into consideration:

Relation (7) is a combination between empirical relations used to calculate the drag coefficient for a solid sphere and a gas bubble; at $Re_2 > 100$, there is little information about the flow past a solid sphere or a gas bubble.

To increase the agreement between the present results and those of relation (7), one can try to change the coefficients of relation (7). However, a fair change of relation (7) should be made, in our opinion, by verifying the relations used to compute the drag coefficient for the flow past a solid sphere and a gas bubble for $Re_2 > 100$. These computations are outside the aims of this paper.

5. Conclusions

The Navier–Stokes equations for steady axisymmetrical flow about a fluid sphere have been solved for moderate Reynolds numbers ($100 \leqslant Re_2 \leqslant 500$) using a finite difference scheme. For each Re_2 value the viscosity and density ratios are varied from 0.01 to 100.

The conclusion frequently encountered in the flow past a fluid particle is, Oliver and Chung (1987) for example, "the flow patterns and the drag coefficient show little variation with the interior Reynolds number." Concerning the drag coefficient the previous statement confirms this. The equation proposed by Rivkind and Ryskin (1976) for predicting the drag coefficient may be considered satisfactory only at $Re_2 = 100$. The strengths of the internal circulation increase with the Reynolds number and decrease with the increase in the viscosity ratio. For a given exterior Re number and Φ_v values, $2 \leqslant \Phi_v < 10$, the variation of the density ratio, and implicitly of the interior Re number, has a significant influence on the exterior flow patterns. This influence is quantified by the flow return behind drop. It is shown that a flow return arises behind the drop in flow without separation.

References

Abdel-Alim, A.H., Hamielec, A.E., 1975. A theoretical and experimental investigation of the effect of internal circulation on the drag of spherical droplets falling at terminal velocity in liquid media. Ind. Eng. Chem. Fundam. 14, 308–312.

Auzinger, W., Stetter, H.J., 1982. Defect correction and multigrid iterations. In: Lecture Notes in Mathematics, vol. 960. Springer, Berlin, pp. 327–351.

Botta, E.F.F., Veldman, A.E.P., 1981. On local relaxation methods and their applications to convection-diffusion equations. J. Comput. Phys. 48, 127–149.

Cliffe, K.A., Lever, D.A., 1986. A comparison of finite-element methods for solving flow past a sphere. J. Comput. Phys. 62, 321–330.

Clift, R., Grace, J.R., Weber, M.E., 1978. Bubbles, Drops and Particles. Academic Press, New York.

Fasel, H.F., 1977. Numerical solution of the complete Navier-Stokes equations for the simulation of unsteady flows. In: Lecture Notes in Mathematics, vol. 771. Springer, Berlin, pp. 177–195.

Gupta, M.M., Manohar, R.P., Stephenson, J.W., 1984. A single cell high order scheme for the convection-diffusion equation with variable coefficients. Int. J. Numer. Meth. Fluids 4, 641–651.

Hackbusch, W., 1985. Multi-Grid Methods and Applications. Springer, Berlin.

Juncu, Gh., Mihail, R., 1989. Numerical experiments with local relaxation and ILU in solving the incompressible Navier–Stokes equations for the flow past a sphere. Unpublished results.

Juncu, Gh., Mihail, R., 1990. Numerical solution of the steady incompressible Navier–Stokes equations for the flow past a sphere by a multigrid defect correction technique. Int. J. Num. Meth. Fluids 11, 379–395.

Oliver, D.L.R., Chung, J.N., 1985. Steady flows inside and around a fluid sphere at low Reynolds numbers. J. Fluid Mech. 154, 215–230.

Oliver, D.L.R., Chung, J.N., 1987. Flow about a fluid sphere at low to moderate Reynolds numbers. J. Fluid Mech. 177, 1–18.

Rivkind, V.Ya., Ryskin, G.M., 1976. Flow structure in motion of a spherical drop in a fluid medium at intermediate Reynolds numbers. Fluid Dyn. 11, 5–12.

Rivkind, V.Y., Ryskin, G.M., Fishbein, G.A., 1976. Flow around a spherical drop at intermediate Reynolds numbers. Appl. Math. Mech. 40, 687–691.

Sadhal, S.S., Ayyaswamy, P.S., Chung, J.N.-C., 1996. Transport Phenomena with Drops and Bubbles. Springer, Berlin.

Stetter, H.J., 1978. The defect correction principle and discretization methods. Numer. Math. 29, 425–443.

Wellek, R.M., Agrawal, A.K., Skelland, H.P., 1966. Shape of liquid drops moving in liquid media. A.I.Ch.E. J. 12, 854–862.